Supporting Information for *Acta Phys. -Chim. Sin.* doi: 10.3866/PKU.WHXB202104003

原位修饰策略实现高倍率室温固态锂电池

赵江辉[1,2,†]，谢茂玲[3,†]，张海洋[2]，易若玮[2]，胡晨吉[2,4]，康拓[2]，郑磊[1,2]，崔瑞广[2]，陈宏伟[3]，沈炎宾[1,2,*]，陈立桅[2,4]

[1] 中国科学技术大学纳米技术与纳米仿生学院，合肥 230026

[2] 中国科学院苏州纳米技术与纳米仿生研究所，国际实验室卓越纳米科学中心，江苏 苏州 215123

[3] 华侨大学材料科学与工程学院，福建 厦门 361021

[4] 上海交通大学化学化工学院，上海 200240

In Situ Modification Strategy for Development of Room-Temperature Solid-State Lithium Batteries with High Rate Capability

Jianghui Zhao[1,2,†], Maoling Xie[3,†], Haiyang Zhang[2], Ruowei Yi[2], Chenji Hu[2,4], Tuo Kang[2], Lei Zheng[1,2], Ruiguang Cui[2], Hongwei Chen[3], Yanbin Shen[1,2,*], Liwei Chen[2,4]

[1] School of Nano-Tech and Nano-Bionics, University of Science and Technology of China, Hefei 230026, China.

[2] i-Lab, CAS Center for Excellence in Nanoscience, Suzhou Institute of Nano-Tech and Nano-Bionics, Chinese Academy of Sciences, Suzhou 215123, Jiangsu Province, China.

[3] College of Materials Science and Engineering, Huaqiao University, Xiamen 361021, Fujian Province, China.

[4] School of Chemistry and Chemical Engineering, Shanghai Jiaotong University, Shanghai 200240, China.

[*]Corresponding author. Email: ybshen2017@sinano.ac.cn; Tel.: +86-512-62872503.

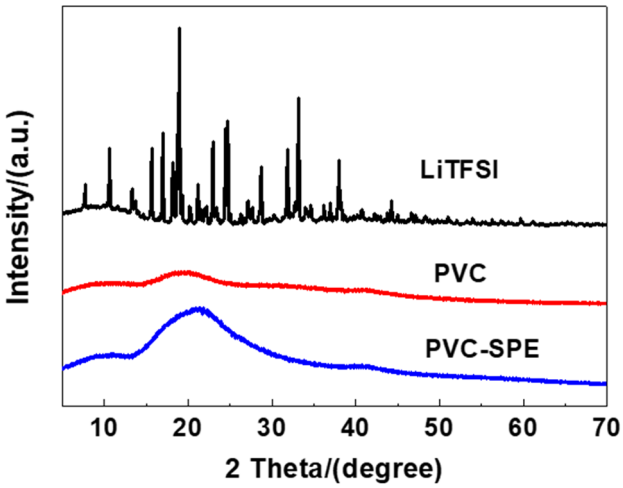

Fig. S1 XRD spectra of LiTFSI, PVC, and PVC-SPE.

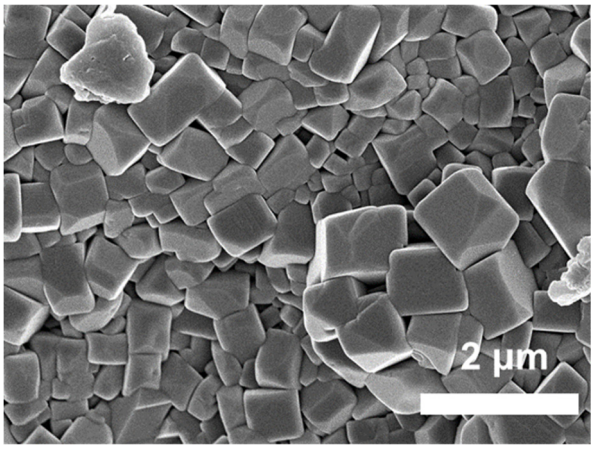

Fig. S2 The SEM images showing the morphology of the pristine LAGP pellet.

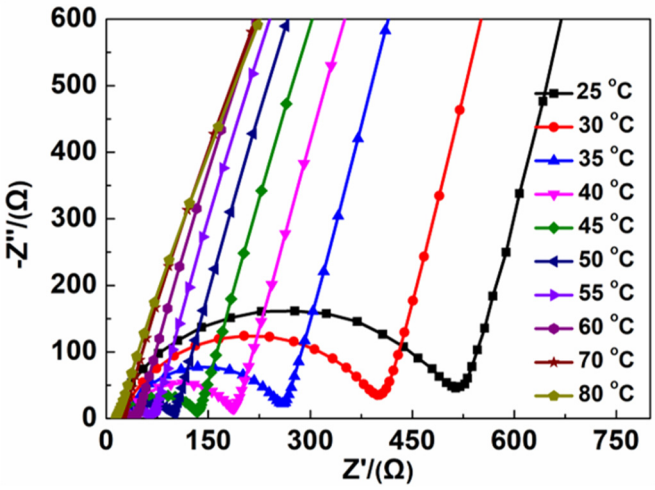

Fig. S3 The corresponding EIS measurements for stainless steel | PVC-SPE | stainless steel cell at different temperatures.

The ionic conductivity (σ) of LAGP electrolyte and PVC-SPE was calculated by Eq. (1):

$$\sigma = \frac{L}{RS} \quad (1)$$

where L is the thickness of electrolyte, R is electrolyte resistance, and S is the contact surface area of the electrolyte and the blocking electrodes.

The lithium-ion transference number (t_{Li^+}) can be calculated by the Bruce-Vincent-Evans technique as Eq. (2):

$$t_{Li^+} = \frac{I_s(\Delta V - I_0 R_0)}{I_0(\Delta V - I_s R_s)} \quad (2)$$

where I_0, I_s are current values measured at the pristine-state and the steady-state condition, respectively; ΔV is a constant DC polarization (5 mV), R_0, R_s are resistance values of initial and steady-state condition, respectively.

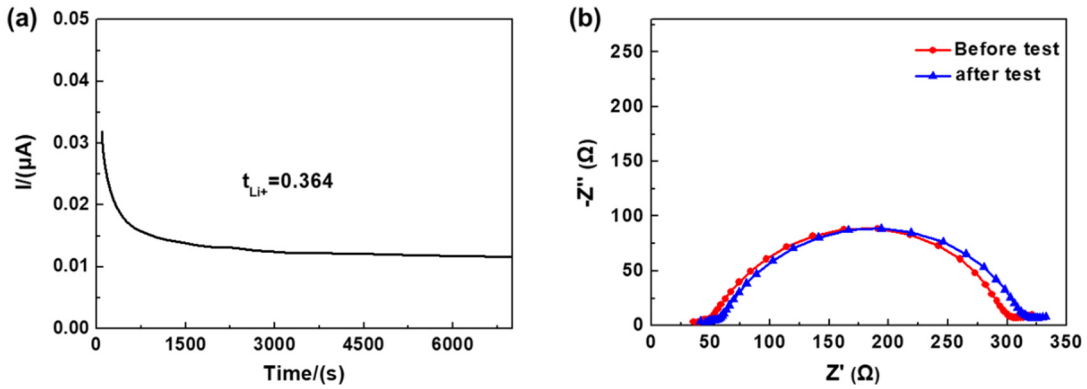

Fig. S4 The chronoamperometry profile of a symmetric Li | PVC-SPE | Li batteries (under 5 mV polarization voltage) at room temperature (a), and the EIS measurements of the symmetrical cell before and after polarization (b).

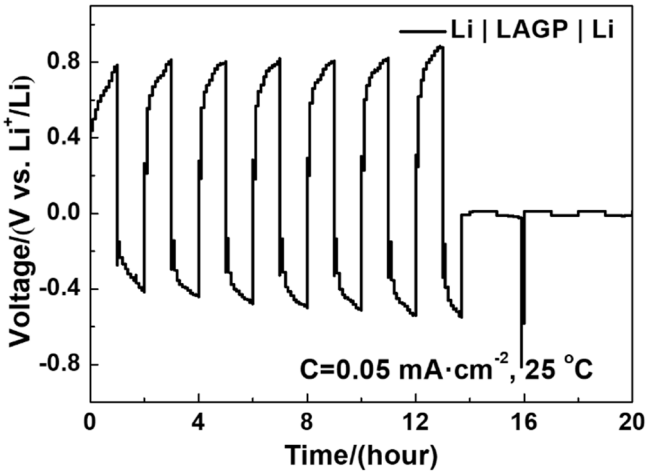

Fig. S5 Voltage profiles of the Li | LAGP | Li battery at a current density of 0.05 mA·cm^{-2} at room temperature.

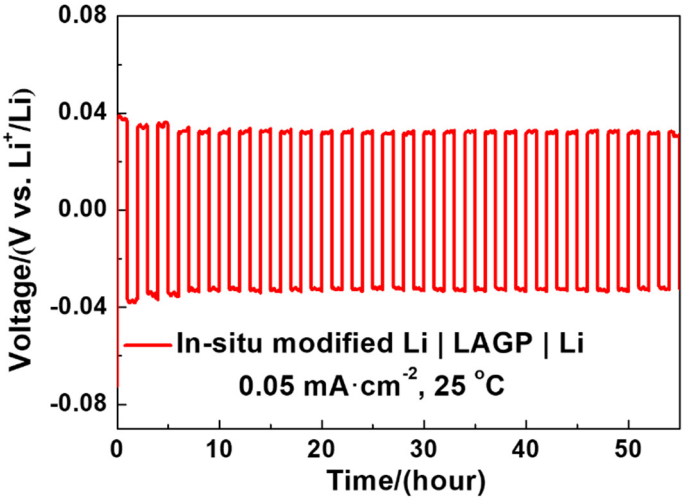

Fig. S6 Voltage profiles of the *in situ* modified Li | LAGP | Li battery at a current density of 0.05 mA·cm^{-2} at room temperature.

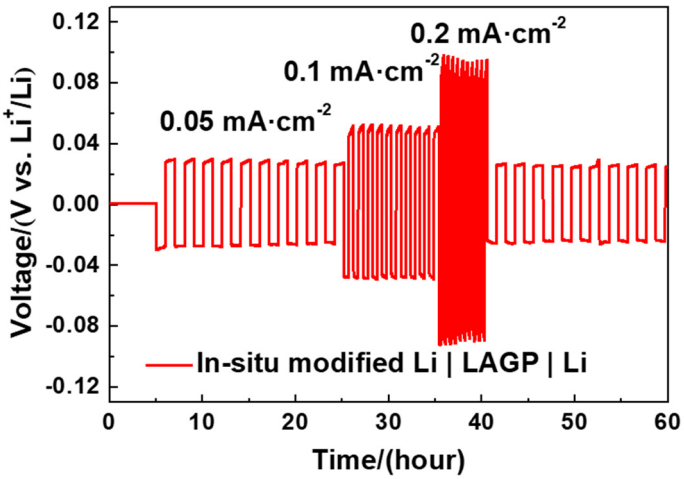

Fig. S7 Voltage profiles of the in-situ modified Li | LAGP | Li battery under different densities of 0.05, 0.1 and 0.2 mA·cm^{-2} at room temperature.

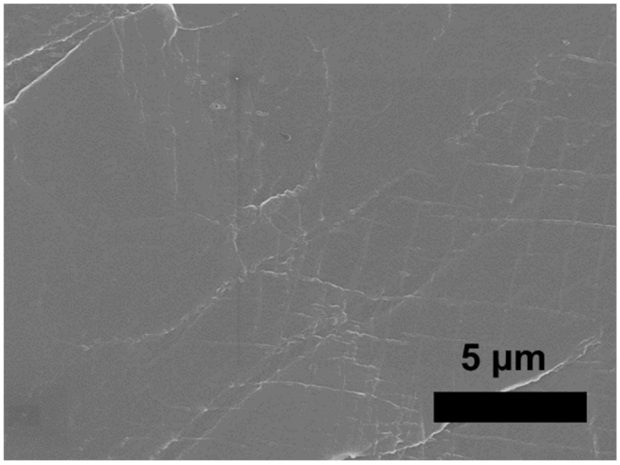

Fig. S8 The SEM images showing the morphology of the pristine Li metal anode.

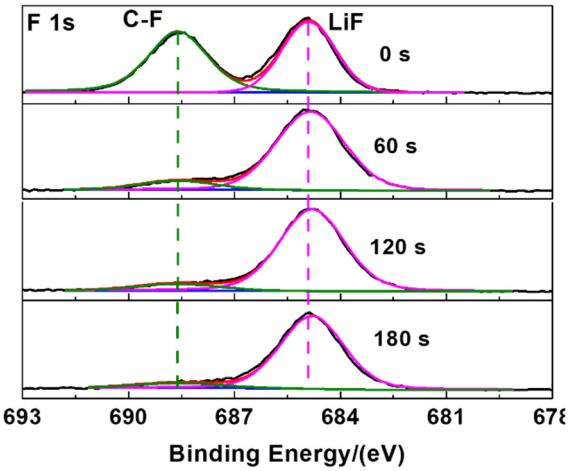

Fig. S9 The in-depth XPS spectra of F 1*s* on the surface of Li metal anodes obtained from *in situ* PVC-SPE modified Li | LAGP | Li cells after 20 cycles.

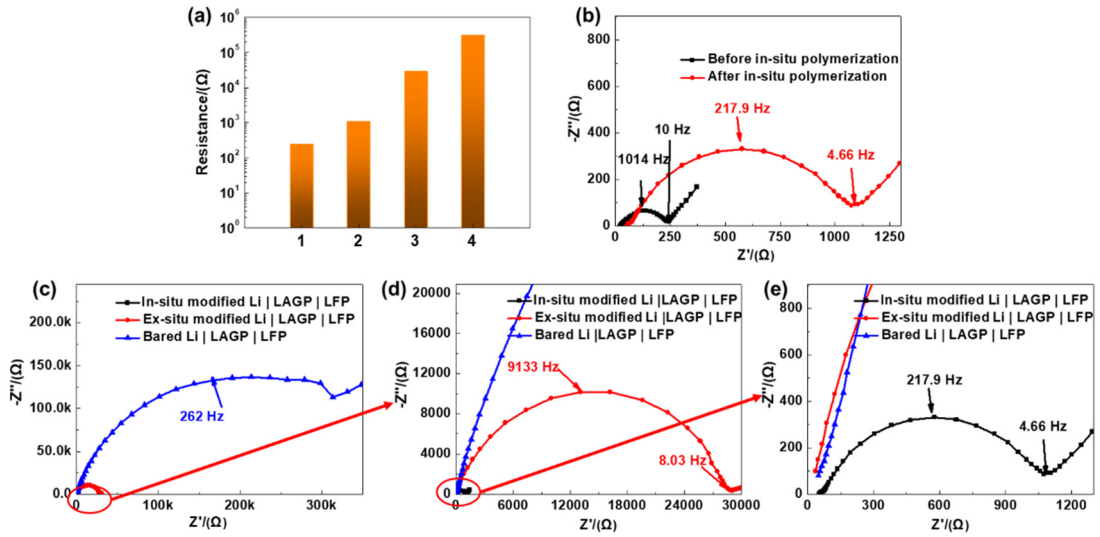

Fig. S10 (a) Impedance of Li | LAGP | $LiFePO_4$ battery at different conditions, 1- before the in-situ polymerization of the PVC-SPE modified Li | LAGP | $LiFePO_4$ battery, 2-after the in-situ polymerization of the PVC-SPE modified Li | LAGP | $LiFePO_4$ battery, 3- Li | LAGP | $LiFePO_4$ cell with *ex-situ* formed PVC-SPE, 4- unmodified Li| LAGP | $LiFePO_4$ cell; (b) the Nyquist plot of PVC-SPE modified Li | LAGP | $LiFePO_4$ battery before and after the in-situ polymerization; (c) the Nyquist plot of the in-situ PVC-SPE modified Li | LAGP| $LiFePO_4$ cell, the ex-situ PVC-SPE modified Li | LAGP | $LiFePO_4$ cell, and the Li | LAGP | $LiFePO_4$ cell at room temperature; (d) the magnified area of Fig. S7(c); (e) the magnified area of Fig. S7(d).

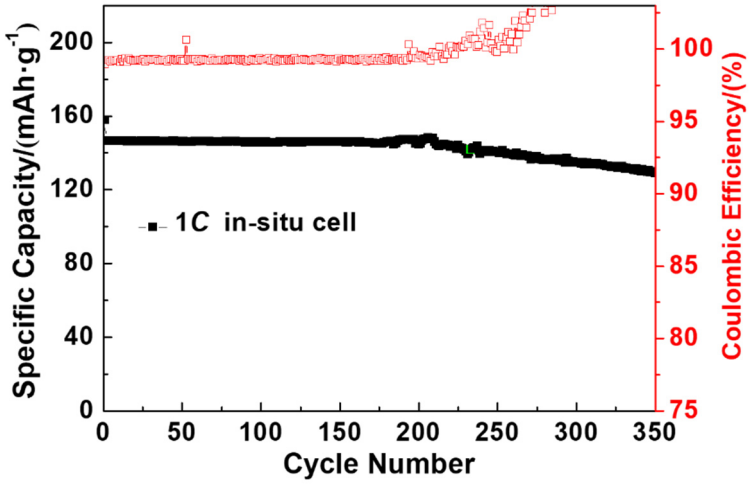

Fig. S11 The long-term cycling performance of the in-situ PVC-SPE modified Li | LAGP | $LiFePO_4$ solid-state battery measured at 1*C* rate.

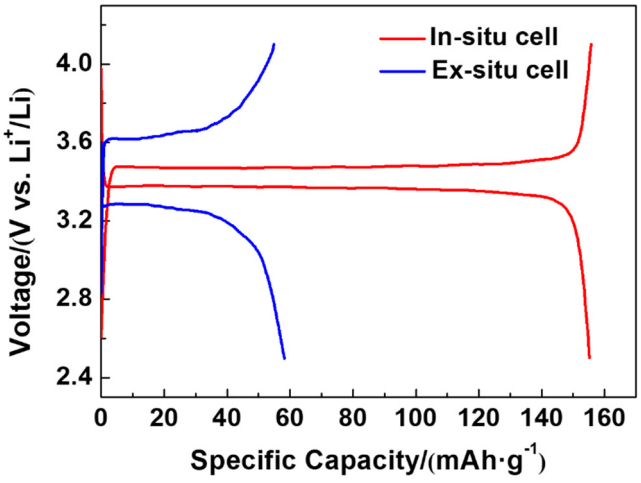

Fig. S12 The galvanostatic charge-discharge profiles of *in situ* PVC-SPE modified Li | LAGP | $LiFePO_4$ battery and *ex-situ* PVC-SPE modified Li | LAGP | $LiFePO_4$ battery at the 2nd cycles.

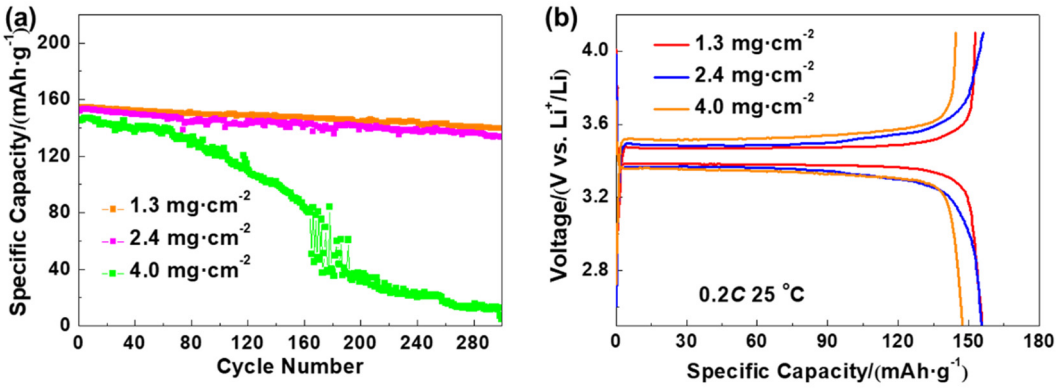

Fig. S13 The long-term cycling performance (a) and the corresponding 2nd cycle voltage profiles; (b) of *in situ* PVC-SPE modified Li | LAGP | $LiFePO_4$ batteries with different active mass loading.

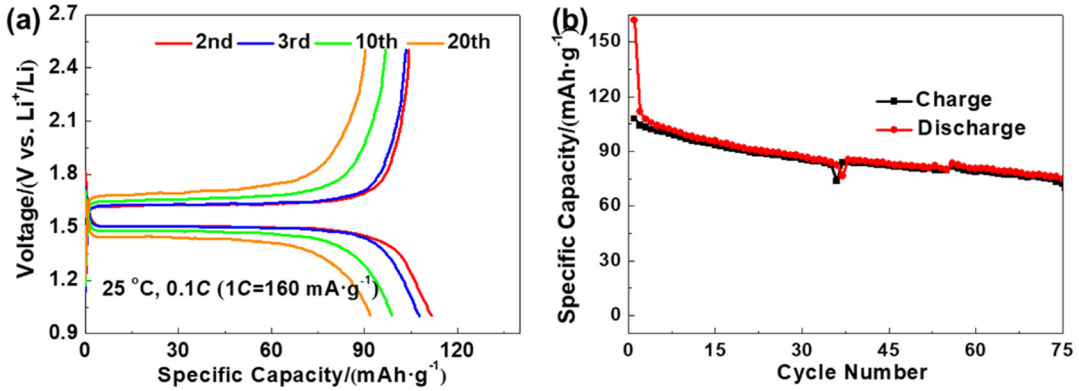

Fig. S14 The evolution of the galvanostatic profile during cycling (a) and the corresponding cycling performance of the *in situ* PVC-SPE modified Li | LAGP | Li_2TiO_3 cell with active mass loading of 1.5 mg·cm^{-2} (b). The current density is 0.1*C* (1*C* = 160 mA·g^{-1}).

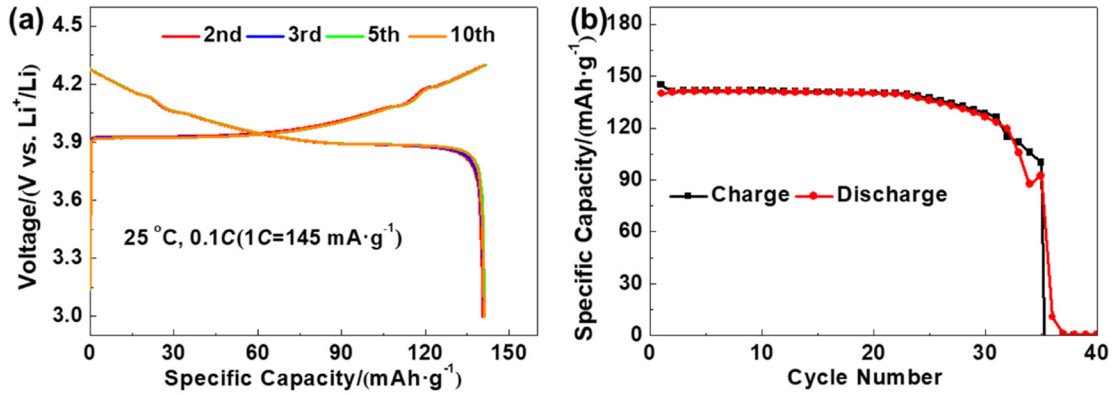

Fig. S15 The evolution of the galvanostatic profile during cycling (a) and the corresponding cycling performance of the *in situ* PVC-SPE modified Li | LAGP | LCO cell with active mass loading of 2 mg·cm^{-2} (b). The current density is 0.1*C* (1*C* = 145 mA·g^{-1}).

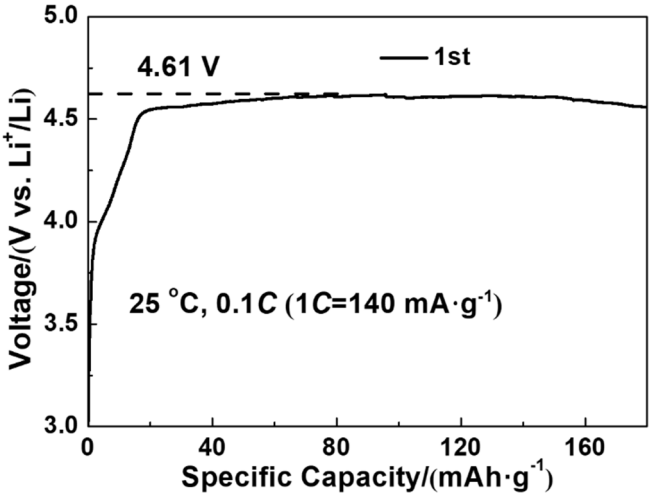

Fig. S16 The initial galvanostatic charging profile of the *in situ* PVC-SPE modified Li | LAGP | $LiNi_{0.5}Mn_{1.5}O_4$ cell at the first cycle. The current density is 0.1*C* (1*C* = 140 mA·g^{-1}).

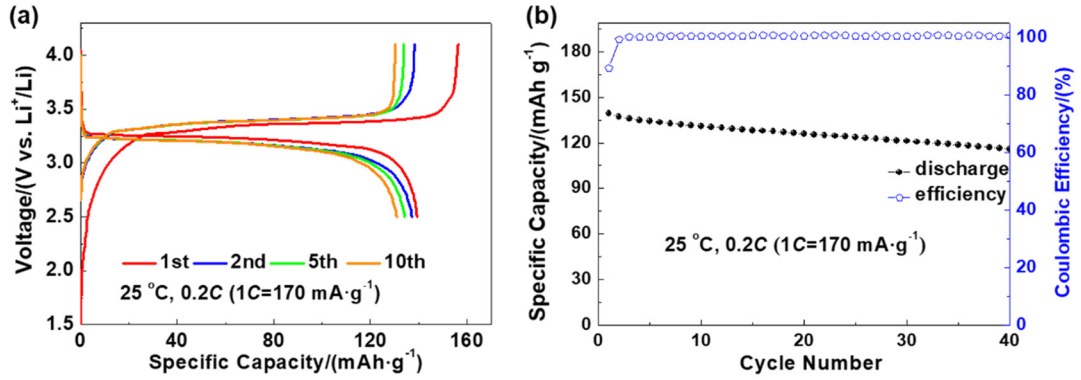

Fig. S17 The evolution of the voltage profile during cycling (a) and cycling performance of the *in situ* PVC-SPE modified graphite |LAGP | $LiFePO_4$ with 4.0 mg·cm^{-2} cell (b).

Table S1 Performance comparison of Li| LAGP| Li symmetric battery with previously published results.

Interface improvement strategy	Current/(mA·cm^{-2})	Overpotential/(mV)	Lifespan (hours)	Work temperature/(℃)	Refs.
in situ modified PVC-SPE	0.05	34	2700	25	This work
electronic conductive graphite layer and composite polymer electrolyte buffer layer	0.1	20	1000	60	1
Bi buffer	0.1	60	300	30	2
C_{60} interlayer	0.1	800	1800	25	3
plastic super-conductive interlayer	0.1	20	400	40	4
ASHE/CHSE double layer	0.1	200	700	25	4
PPC-SPEs	0.05	55	200	55	5
CuF_2 layer	0.1	80	1500	25	6
LAGP nanoparticles/ionic liquid layer	0.1	30	1500	25	7
PVC-TPU layer	0.1	100	1000	25	8
TMP/FEC	0.1	＜120	1000	25	9

Table S2 Comparison of the cycling performance of Li| LAGP| cathode batteries with previously published results.

Electrode	Interface improvement strategy	Ionic conducted addictive in electrode	Rate performance	Cycling performance	Refs.
$LiFePO_4$	in situ modified PVC-SPE	in situ modified PVC-SPE	72.4% (3*C*)	98% (200 cycles)	This work
$LiFePO_4$	N/A	PVDF-LiTFSI	N/A	28.5%（50 cycles）	10
$LiFePO_4$	electronic conductive graphite layer and composite polymer electrolyte buffer layer	Ex situ CPE	N/A	96% (100cycles) (60 °C)	1
$LiFePO_4$	Bi buffer	5 μL liquid electrolyte	N/A	≈ 100%（120 cycles）	2
$LiFePO_4$	C_{60} interlayer	5 μL liquid electrolyte	89.4% (0.6*C*)	85% (100 cycles)	3
$LiFePO_4$	plastic super-conductive interlayer	plastic super-conductive interlayer	69.5% (1*C*)	93.17% (100 cycles) (40 °C)	4
$LiMn_2O_4$	ASHE/CHSE double layer	5 μL liquid electrolyte	64.3% (0.5*C*)	74.2% (120 cycles)	4
$LiFePO_4$	PPC-SPEs	PPC-SPEs/LAGP	50.4% (1*C*) (55 °C)	71% (90 cycles) (55 °C)	5
S cathode	CuF_2 layer	2 μL liquid electrolyte	N/A	79.8% (50 cycles)	6
$LiFePO_4$	LAGP nanoparticles/ionic liquid layer	5 μL liquid electrolyte	73% (2*C*)	80.4% (200 cycles)	7
$LiFePO_4$	PVC−TPU layer	Ex situ PVC-TPU	N/A	95.3% (100 cycles)	8
$LiFePO_4$	TMP/FEC	LAGP	74.6% (2*C*)	80% (700 cycles)	9
Li-O_2			N/A	Stable cycling 500 cycles	

Table S3 Comparison of the cycling performance of in situ solid batteries with previously published results.

Electrode	Electrolyte	Rate performance	Cycling retention	Refs.
$LiFePO_4$	In situ modified LAGP	72.4% (3*C*)	98% (200 cycles)	The work
$LiCoO_2$	In situ PVC SPE	64% (0.5*C*)	84.2% (150 cycles) (50 °C)	11
$LiFePO_4$	In situ DOL electrolyte	none	87.5% (700 cycles)	1
$LiFePO_4$	In situ TSPE electrolyte	42.8% (5*C*)	80% (400 cycles) (30 °C)	12
$NaNi_{1/3}Fe_{1/3}Mn_{1/3}O_2$	In situ PVC SPE	59.1% (5*C*)	86.8% (250 cycles)	13
$LiFePO_4$	In situ PTHF SPE	none	91.3%(100 cycles) (60 °C)	14
$LiFePO_4$	In situ C-PEGDE	59.2% (0.2*C*)	74.2% (100 cycles)	15
$LiFePO_4$	In situ DN-SPE	none	99.5% (150 cycles) (55 °C)	16
$LiFePO_4$	VC-PEGMA SPE	90% (0.5*C*)	68% (600 cycles) (60 °C)	3
$Na_3V_2(PO_4)_3$	PEGDMA SPE	84% (1*C*)	95% (740 cycles) (60 °C)	17
$LiFePO_4$	HPILSE	50% (1*C*)	97.7% (100 cycles)	18

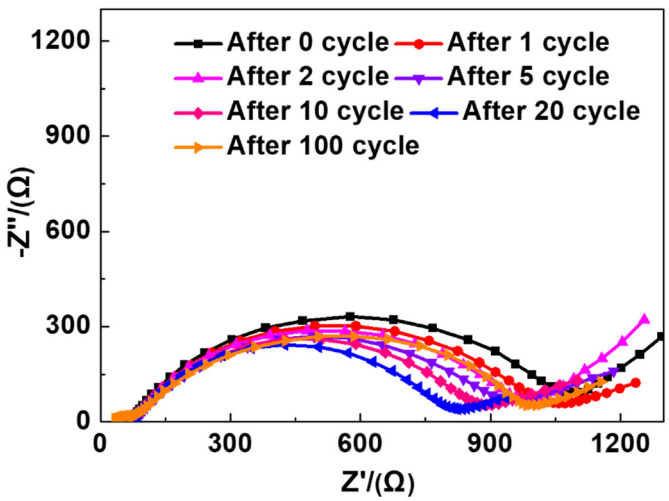

Fig. S18 The impedance of the in-situ modified Li | LAGP | $LiFePO_4$ cell after different cycles at room temperature.

References

(1) Li, W.; Wang, Q.; Jin, J.; Li, Y.; Wu, M.; Wen, Z. *Energy Storage Mater.* **2019,** *23*, 299. doi: 10.1016/j.ensm.2019.04.044

(2) Hu, F.; Li, Y.; Wei, Y.; Yang, J.; Hu, P.; Rao, Z.; Chen, X.; Yuan, L.; Li, Z. *ACS Appl Mater Interfaces* **2020,** *12*, 12793. doi: 10.1021/acsami.9b21717

(3) Zhao, Y.; Bai, Y.; Liu, A.; Li, W.; An, M.; Bai, Y.; Chen, G. *J. Power Sources* **2020,** *450*, 227614. doi: 10.1016/j.jpowsour.2019.227614

(4) Liu, Q.; Zhou, D.; Shanmukaraj, D.; Li, P.; Kang, F.; Li, B.; Armand, M.; Wang, G., *ACS Energy Lett.* **2020,** *5*, 1456. doi: 10.1021/acsenergylett.0c00542

(5) Wang, L.; Liu, D.; Huang, T.; Geng, Z.; Yu, A. *RSC Advances* **2020,** *10*, 10038. doi: 10.1039/d0ra00829j

(6) Wei, Y.; Hu, F.; Li, Y.; Yang, J.; Wang, W.; Yuan, L.; Zhang, W.; Li, Z.; Huang, Y. *ACS Appl Mater Interfaces* **2020,** *12*, 39335. doi: 10.1021/acsami.0c11761

(7) Xiong, S.; Liu, Y.; Jankowski, P.; Liu, Q.; Nitze, F.; Xie, K.; Song, J.; Matic, A. *Adv. Funct. Mater.* **2020,** *30*, 2001444. doi: 10.1002/adfm.202001444

(8) Zhai, P.; Fu, L.; Yuan, S.; Shi, L.; Zhu, J.; Zhao, Y.; Wang, Z. *ACS Appl. Energy Mater.* **2020,** *3*, 7011. doi: 10.1021/acsaem.0c01065

(9) Zou, X.; Lu, Q.; Zhang, X.; Ran, R.; Zhou, W.; Liao, K.; Shao, Z. *Energy Fuels* **2020,** *34*, 11547. doi: 10.1021/acs.energyfuels.0c02222

(10) Meesala, Y.; Chen, C. Y.; Jena, A.; Liao, Y. K.; Hu, S. F.; Chang, H.; Liu, R. S. *J. Phys. Chem. C* **2018,** *122*, 14383. doi: 10.1021/acs.jpcc.8b03971

(11) Chai, J.; Liu, Z.; Ma, J.; Wang, J.; Liu, X.; Liu, H.; Zhang, J.; Cui, G.; Chen, L. *Adv. Sci.* **2017,** *4*, 1600377. doi: 10.1002/advs.201600377

(12) Zhou, J.; Qian, T.; Liu, J.; Wang, M.; Zhang, L.; Yan, C. *Nano Lett.* **2019,** *19*, 3066. doi: 10.1021/acs.nanolett.9b00450

(13) Chen, S.; Che, H.; Feng, F.; Liao, J.; Wang, H.; Yin, Y.; Ma, Z. F. *ACS Appl. Mater. Inter.* **2019,** *11*, 43056. doi: 10.1021/acsami.9b11259

(14) Huang, S.; Cui, Z.; Qiao, L.; Xu, G.; Zhang, J.; Tang, K.; Liu, X.; Wang, Q.; Zhou, X.; Zhang, B.; *et al*. *Electrochim. Acta* **2019,** *299*, 820. doi: 10.1016/j.electacta.2019.01.039

(15) Cui, Y.; Liang, X.; Chai, J.; Cui, Z.; Wang, Q.; He, W.; Liu, X.; Liu, Z.; Cui, G.; Feng, J., *Adv. Sci.* **2017,** *4*, 1700174. doi: 10.1002/advs.201700174

(16) Duan, H.; Yin, Y. X.; Zeng, X. X.; Li, J. Y.; Shi, J. L.; Shi, Y.; Wen, R.; Guo, Y. G.; Wan, L. J., *Energy Storage Mater.* **2018,** *10*, 85. doi: 10.1016/j.ensm.2017.06.017

(17) Yao, Y.; Wei, Z.; Wang, H.; Huang, H.; Jiang, Y.; Wu, X.; Yao, X.; Wu, Z. S.; Yu, Y., *Adv. Energy Mater.* **2020,** *10*, 1903698. doi: 10.1002/aenm.201903698

(18) Zhou, D.; Liu, R.; Zhang, J.; Qi, X.; He, Y. B.; Li, B.; Yang, Q. H.; Hu, Y. S.; Kang, F., *Nano Energy* **2017,** *33*, 45. doi: 10.1016/j.nanoen.2017.01.027